Hand-In Tasks on Semiconductor Detectors

Alexander Burgman
Nov 2015 – Jan 2016

1 Part 1 — *From the Exercise Session*

1.1 PN-Diode

The initial conditions used to simulate the pn-diode can be found in Tab. 1.1.

Material	Temperature (K)	Acceptor Concentration (cm^{-3})	Donor Concentration (cm^{-3})
Si	273	10^{16}	10^{16}
		10^{15}	10^{17}
	293	10^{16}	10^{16}
		10^{15}	10^{17}
	313	10^{16}	10^{16}
		10^{15}	10^{17}
Ge	273	10^{16}	10^{16}
		10^{15}	10^{17}
	293	10^{16}	10^{16}
		10^{15}	10^{17}
	313	10^{16}	10^{16}
		10^{15}	10^{17}

Table 1.1: The initial conditions for which the pn-diode was simulated.

The result of the simulation can be found in Fig. 1.2. Here, the electric field E and potential Ψ are displayed over the entire length of the diode (on the x axis). The numbers noted in italics in the legend, X-Y, denote the acceptor and donor number densities, where X-Y corresponds to an acceptor number density $N_A = 10^X$ cm^{-3} and donor number density $N_D = 10^Y$ cm^{-3}.

It is evident that a symmetric doping (i.e. $X = Y$) yields symmetry both in the potential and electric field, while an asymmetric doping (i.e. $X \neq Y$) yields asymmetry in both. From the lecture notes it is clear that the electric field will be more present in the more heavily doped region than the more lightly doped region, which can also be observed in the simulation results. Additionally, it was found that the potential magnitude decreased with increasing temperature, and that the potential was shifted towards its mean value with increasing temperature (i.e. the higher part of the potential was shifted downwards and the lower part of the potential was shifted upwards).

The potential difference between the donor and acceptor regions is called the built in potential, Ψ_0. The built in potential is calculated from Eq. 1.1.

$$\Psi_0 = \frac{k_B T}{q} \times \ln\left(\frac{N_A N_D}{n_i^2}\right) \tag{1.1}$$

where $k_B = 1.381 \times 10^{-23}$ J/K is the Boltzmann constant, T is the temperature, q is the charge of the charge carriers (here the elementary charge of the electron, $q = e = 1.609 \times 10^{-19}$ C) and n_i is the ~~bulk~~ concentration

intrinsic

of charge carriers. The simulated and theoretically calculated values for the potential in the silicon pn-devices can be found in Tab. 1.2. The same value for n_i is used in all cases, $n_i = 1.5 \times 10^{10}$ cm^{-3}, which is true for silicon at $T = 300$ K.

Material	Temperature (K)	X–Y	Simulated Potential Ψ (V)	Calculated Potential Ψ_0 (V)
Si	273	16–16	0.762	0.628
		15–17	0.719	0.628
	293	16–16	0.723	0.674
		15–17	0.685	0.674
	313	16–16	0.684	0.721
		15–17	0.650	0.721

Table 1.2: The simulated and calculated potentials of the Si diode.

It is clear that the theoretical calculation yields potentials within the same range as the simulation does. However, the calculated values for the potential increase proportionally with increasing temperature whereas the simulated values decrease with increasing temperature. It is possible that this discrepancy comes from a hidden temperature dependence in n_i, as the same value for n_i was used in all calculations here. This temperature dependence would, however, have to be exponential to counteract the factor T, as n_i^2 enters logarithmically. Additionally, the theoretical values predict no difference between the symmetrically and asymmetrically doped cases (with the values used here) whereas the simulation yields a consistently lower potential for the asymmetric case than the symmetric case.

correct!
n(i)=sqrt[N(c)N(V)]e^(-E(g)/2kT)

The calculated potential can also be used to find the depletion width (see Eq. 1.2 [1]).

$$W = \sqrt{\frac{2\epsilon_0 \epsilon_R \Psi_0}{q}\left(\frac{1}{N_A} + \frac{1}{N_D}\right)} \tag{1.2}$$

Here, $q = e$, the vacuum permittivity $\epsilon_0 = 8.85 \times 10^{-12}$ F/m and the relative permittivity for Si is $\epsilon_R = 11.9$ [2].

The calculated widths are shown in Tab. 1.3 along with the simulated widths. Here, the simulated width is defined as the width of the region where the electric field has a value $E(x)$ that fulfills $E(x) > 10^{-3} E_{max}$. At the relevant values of x the simulation evaluates the E-field at each 0.1 μm which is why the widths presented here are no more exact than this.

Material	Temperature (K)	X–Y	Simulated Width W (μm)	Calculated Width W (μm)
Si	273	16–16	0.8	0.406
		15–17	1.4	0.911
	293	16–16	0.8	0.420
		15–17	1.4	0.944
	313	16–16	0.8	0.434
		15–17	1.4	0.976

Table 1.3: The simulated and calculated depletion widths of the Si diode.

The simulated and calculated widths agree to the extent of being of the same order of magnitude, but not much better. However, in both the simulated and calculated values it is clear that the asymmetrically doped diode has a larger width than the symmetrically doped one. The discrepancy could be related to the somewhat arbitrary definition of the simulated width.

Next, a new diode was simulated, of (n+)(n)(p+) type. A bias was put over this diode in order to find the depletion voltage. The IV curves can be found in Fig. 1.1. Here it is clear that each diode has a depletion voltage

Information missing on doping concentration of the regions and geometry.

of around 10 V, that higher temperature allows for a higher current throughput, and that a germanium diode lets through much more current than a silicon diode does.

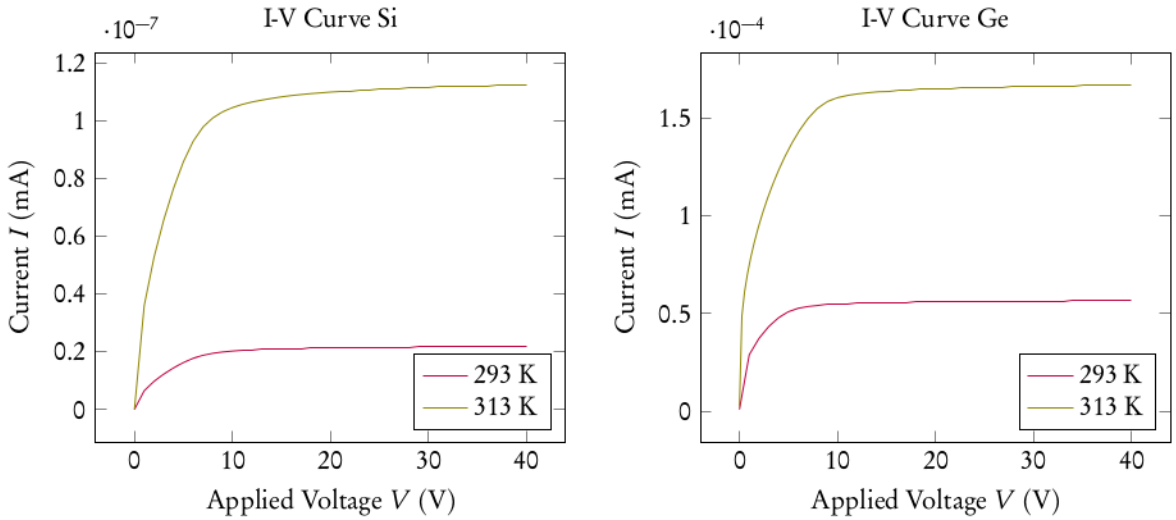

Figure 1.1: The current-voltage curves over a germanium pn-diode and a silicon pn-diode.

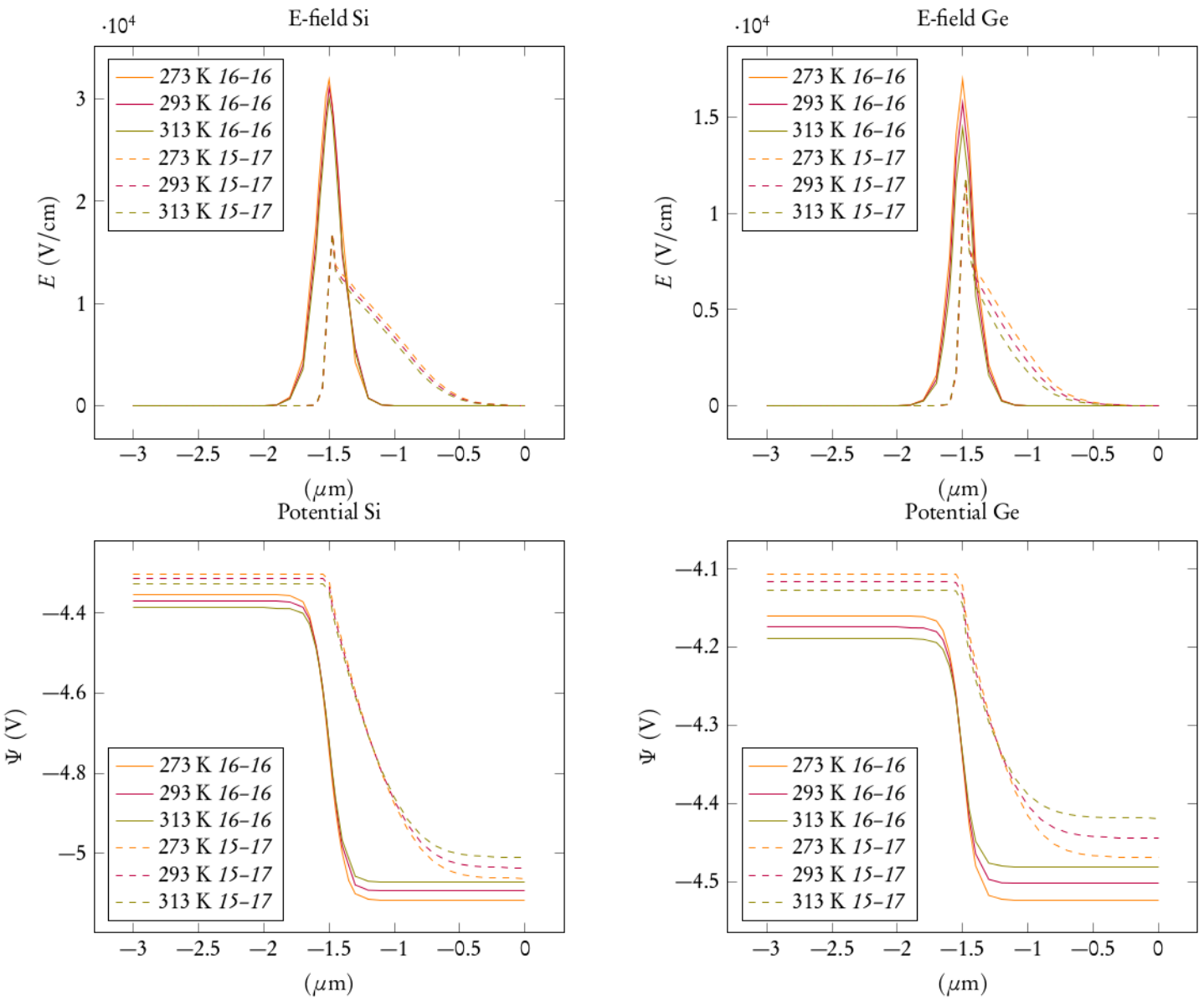

Figure 1.2: The electric field and potential in the silicon and germanium PN diodes. 'X–Y' corresponds to acceptor and donor number densities of 10^X cm^{-3} and 10^Y cm^{-3}. This is shown over the entire PN diode length from —3 μm to 0 μm. The donor region lies between —3 μm and —1.5 μm and the acceptor region lies between —1.5 μm and 0 μm.

1.2 Schottky Diode

The initial conditions used to simulate the Schottky diode can be found in Tab. 1.4.

Material	Temperature (K)	Bulk Acceptor Concentration (cm^{-3})
Si	293	10^{15}
		10^{16}
	313	10^{15}
Ge	293	10^{15}
		10^{16}
	313	10^{15}

Table 1.4: The initial conditions for which the Schottky diode was simulated.

The result of the simulation can be found in Fig. 1.4. Here, the electric field E and potential Ψ are displayed over the entire length of the diode (on the x axis). The number noted in italics in the legend, X, denotes the bulk acceptor number density, where X corresponds to an acceptor number density of 10^X cm^{-3}.

It is evident that a a change in temperature from 20° C to 40° C does not have a significant effect on neither the electric field nor the potential, for either material. The change in acceptor concentration seems to have a larger effect, narrowing the depletion region.

The potential and maximum electric field are in similar ranges for the two types of diodes.

Next, a new Schottky diode was simulated, of dimensions 50 μm × 50 μm. A bias was put over this diode ranging from 0 V to 40 V. The resulting IV curves can be found in Fig. 1.3. The current throughput is similar for both materials and both temperatures in this range of bias voltage. The Schottky diode does not, however, deplete in this voltage range, and the measured currents are many orders of magnitude higher than for the pn-diode treated above.

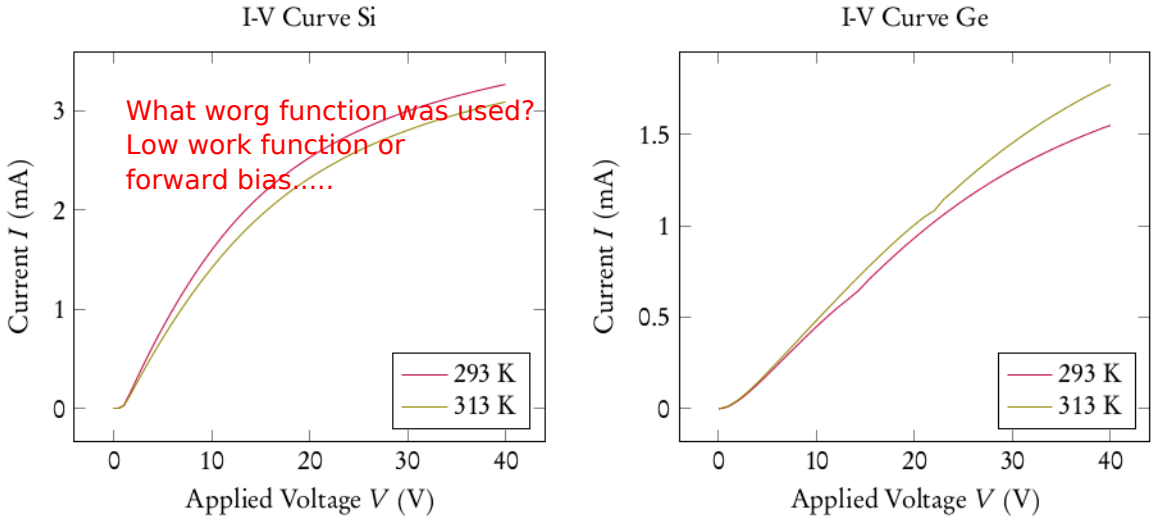

Figure 1.3: The current-voltage curves over a germanium Schottky diode and a silicon Schottky diode.

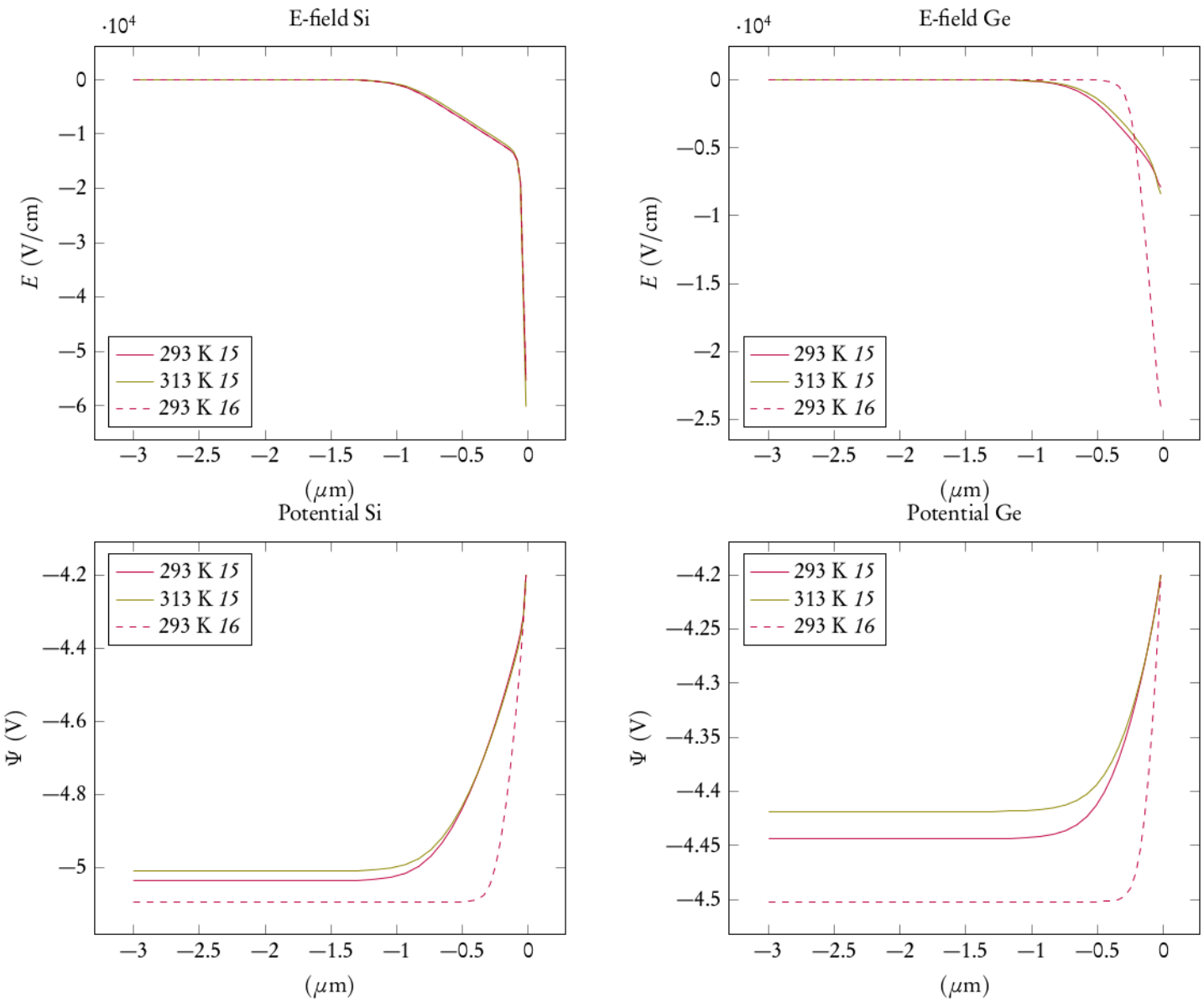

Figure 1.4: The electric field and potential in the silicon and germanium Schottky diodes. The number given in italics 'X' corresponds to the bulk acceptor number density 10^X cm^{-3}. This is shown over the entire Schottky diode length from −3 μm to 0 μm. The metal end-plate is located at 0 μm.

2 Part 2 — *Laboratory Exercise*

2.1 Preamplifier Characterization

Note: this laboratory exercise was done in common in a group of four. This means that all data and all plots shown here are common for all members of the group. The members of this group are Alexander Burgman, Max Isacson, Mikael Mårtensson and Henrik Öhman.

The injected charge Q into the preamplifier is found from Eq. 2.1:

$$Q = C_{cal} \times V \tag{2.1}$$

for a given applied voltage V and where the capacitance $C_{cal} = 0.4$ pF. Applying a voltage $V = 10$ mV yields:

$$Q = 10 \text{ mV} \times 0.4 \text{ pF} = 4 \text{ fC} \approx 25000\, e$$

where e is the elementary charge.

The amplitude, rise time and noise of the preamplifier output were studied for different capacitive loads C_{load}. This was done using an oscilloscope and yielded the values in Tab. 2.1:

rms ?

C_{load} (pF)	Amplitude (mV)	Rise Time (ns)	Noise (μV)	Noise FWHM (μV)
1	40.0	28.1	169	40
4.7	40.1	30.5	182	46
10	38.9	32.5	194	48
27	33.3	39.3	212	45
54	27.3	50.5	247	51
100	20.3	56.9	291	62

?

This is the number to use...

Table 2.1: The amplitude, rise time and noise measured for different values of C_{load}.

The amplitude, rise time and noise can also be seen as functions of the capacitive load in Fig. 2.1, 2.2 and 2.3 respectively. Additionally, Fig. 2.4 displays the calculated ENC (equivalent noise charge) as a function of the capacitive load.

In Fig. 2.3 and 2.4 three additional data points are included. One corresponds to the noise or ENC with no capacitive load attached and the other two correspond to the noise or ENC with a shaping pulse applied. The ENC was measured at a value of 452 e with no capacitive load attached.

Fig. 2.4 also includes a linear fit with a slope of $3.05 \pm 0.11\, e/\text{pF}$. The fit crosses $C_{load} = 0$ at an ENC of $438 \pm 13\, e$, i.e. $\sim 1\sigma$ below the measured value

The equivalent noise charge was trivially calculated from the noise using a modification of Eq. 2.1:

$$Q_{ENC} = C_{cal} \times V_{Noise} \tag{2.2}$$

Q(ENC)= Q* (Noise(rms)/Amplitude)

where Q_{ENC} and V_{Noise} represent the ENC and noise respectively.

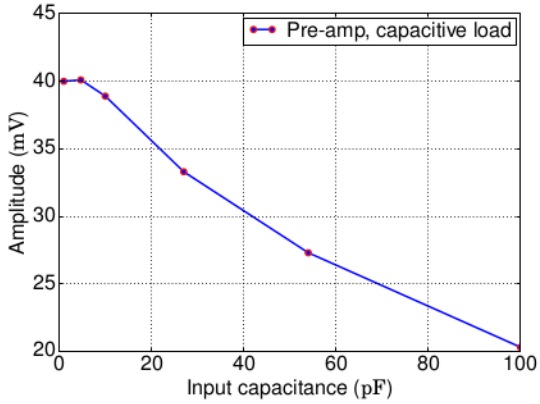

Figure 2.1: The measured amplitude as a function of the capacitive load.

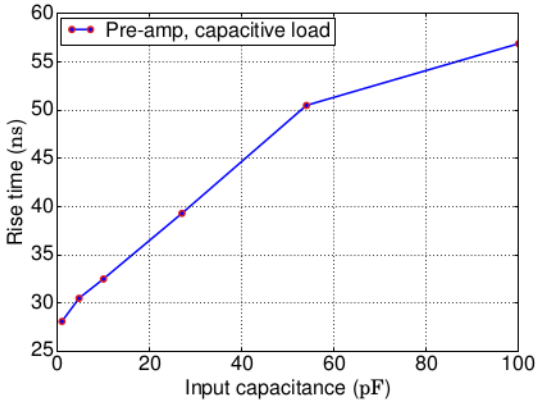

Figure 2.2: The measured rise time as a function of the capacitive load.

wrong calculation of ENC in plot!!!

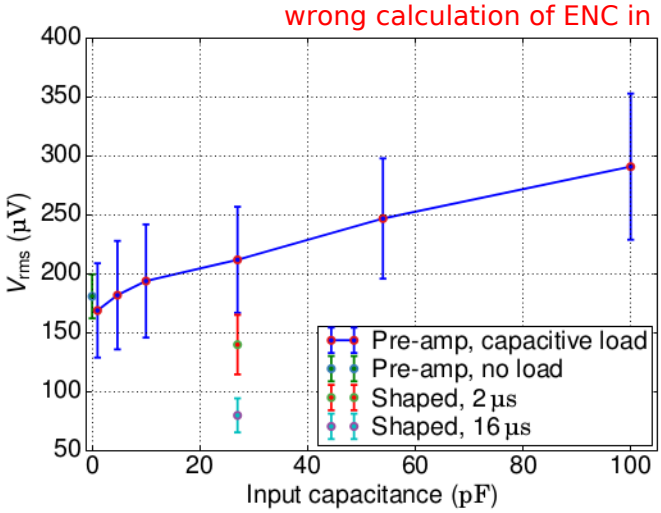

Figure 2.3: The measured noise as a function of the capacitive load. A measurement of the noise with no capacitive load attached is included as well as two points displaying the noise with a shaping pulse applied.

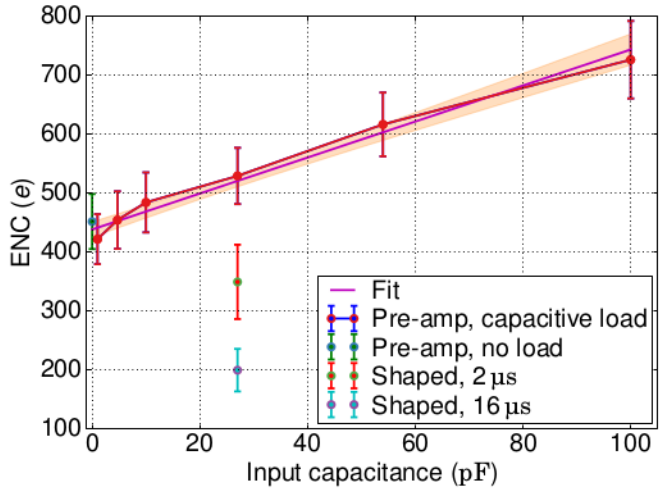

ENC: 100pF -> 358
27pF -> 159

Figure 2.4: The equivalent noise charge as a function of the capacitive load, calculated from the measured noise. A measurement of the ENC with no capacitive load attached is included as well as two points displaying the ENC with a shaping pulse applied.

How did you convert noise with shaping to ENC in your plot? FWHM -> RMS?

2.2 Calibration

In order to translate the channel number of an MCA output to the collected charge a known charge must be detected and the resulting channel number recorded.

This was done for three combinations of gain and shaper time (see Tab. 2.2).

Shaper Time (μs)	Gain
2	100
16	100
16	500

Table 2.2: The shaper time and gain combinations used for the calibration spectrum.

Fig. 2.5 displays the recorded spectra for each of the three shaper time and gain combinations. The three peaks with the highest channel number where used to make a calibration curve for each combination. These can be found in Fig. 2.6, 2.7 and 2.8, along with linear fits.

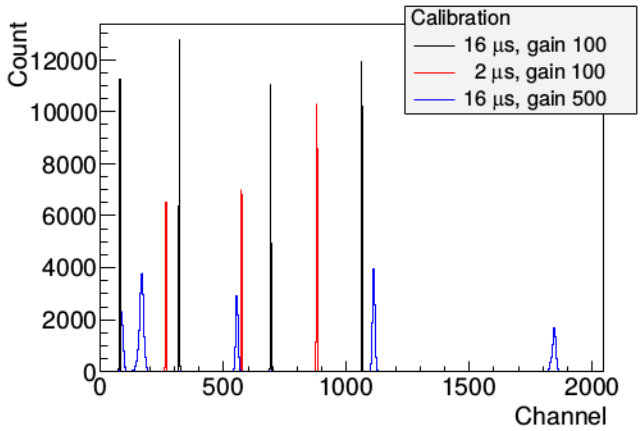

Figure 2.5: The recorded spectra for each of the three shaper time and gain combinations.

The parameters of the linear fits can also be found in Tab. 2.3.

Shaper Time (μs)	Gain	Slope (pC/[channel number])	Offset (pC)
2	100	1.322×10^{-5}	3.043×10^{-4}
16	100	1.086×10^{-5}	4.312×10^{-4}
16	500	1.860×10^{-6}	2.637×10^{-4}

Table 2.3: The linear fit parameters for each combination of shaper time and gain.

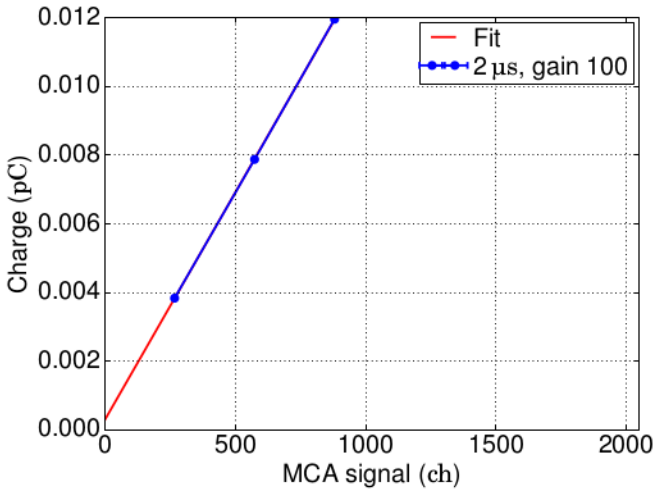

Figure 2.6: The calibration curve for a shaping time of 2 µs and a gain of 100, including a linear fit.

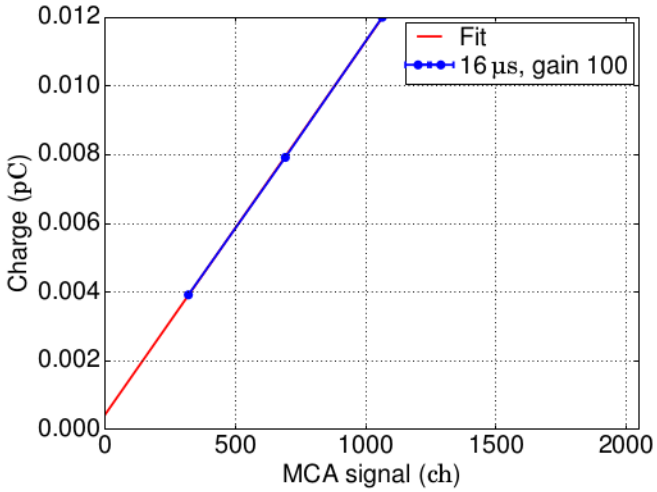

Figure 2.7: The calibration curve for a shaping time of 16 µs and a gain of 100, including a linear fit.

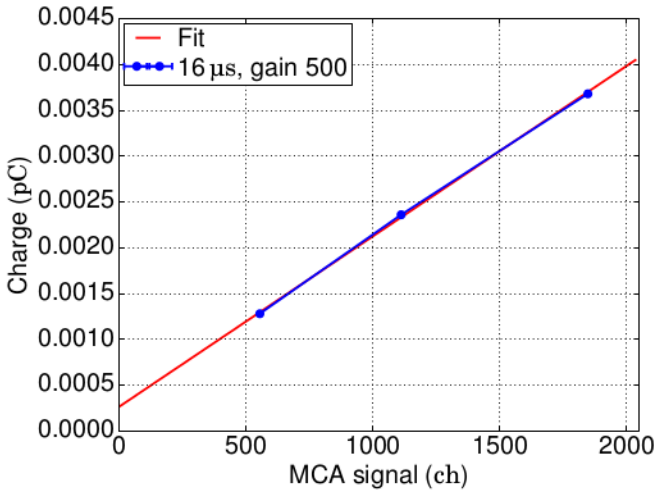

Figure 2.8: The calibration curve for a shaping time of 16 µs and a gain of 500, including a linear fit.

2.3 Source Spectra

Lastly, the spectra of ^{137}Cs and ^{241}Am were measured with the diode. The measured spectrum of ^{137}Cs is shown in Fig. 2.9 and the measured spectrum of ^{241}Am is shown in Fig. 2.10. Additionally, the spectrum of ^{241}Am is shown over the collected charge in Fig. 2.11 where the prominent peak has been fitted with a Gaussian over a first order polynomial background. The mean and RMS of the Gaussian fit were 0.330 fC and 0.0227 fC respectively.

^{241}Am alpha-decays to ^{237}Np* which in turn deexcites by emitting a gamma ray. The alpha particle has an energy 5.49 MeV (84.8%) or 5.44 MeV (13.1%) yielding gamma ray energies of 59.5 keV or 103 keV respectively [3]. The prominent peak found here in the ^{241}Am spectrum is produced by the 59.5 keV gamma ray.

Do you remember the value of the applied revers bias voltage?

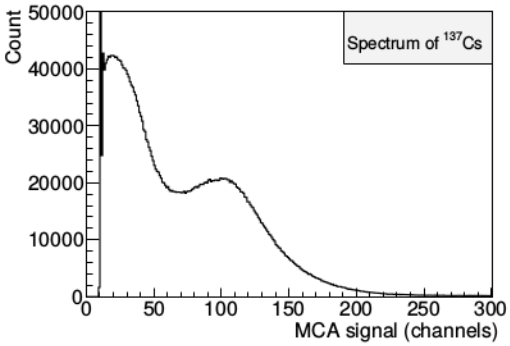

Figure 2.9: The measured spectrum of ^{137}Cs.

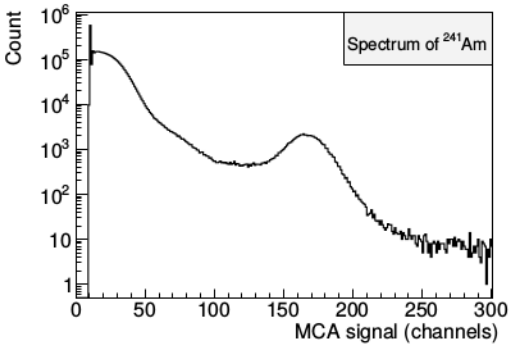

Figure 2.10: The measured spectrum of ^{241}Am.

[1cm]

Fantastic!!!

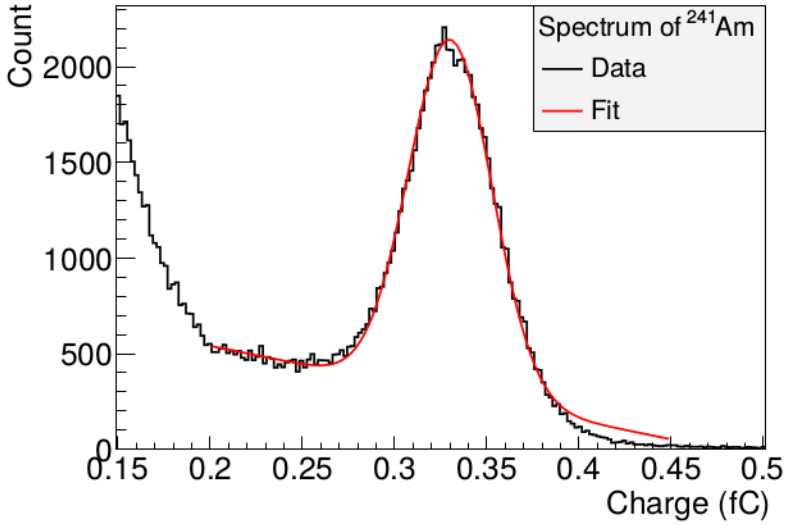

Figure 2.11: The measured spectrum of ^{241}Am over the collected charge. The prominent peak has been fitted with a Gaussian over a first order polynomial background.

3 Part 3 — *Final Simulation and Comparison with Clean Room Measurement*

A simulation was made of the pn-device measured during the clean room exercise in Helsinki. The geometry of the diode was simplified for computational reasons (see Fig. 3.1). As the diode was simulated with a width of 50 μm while the real width was 5 mm, the current output from the simulation was multiplied by a factor of $\frac{5\text{ mm}}{50\ \mu\text{m}} = 100$. The length of the diode was set to be 5 mm.

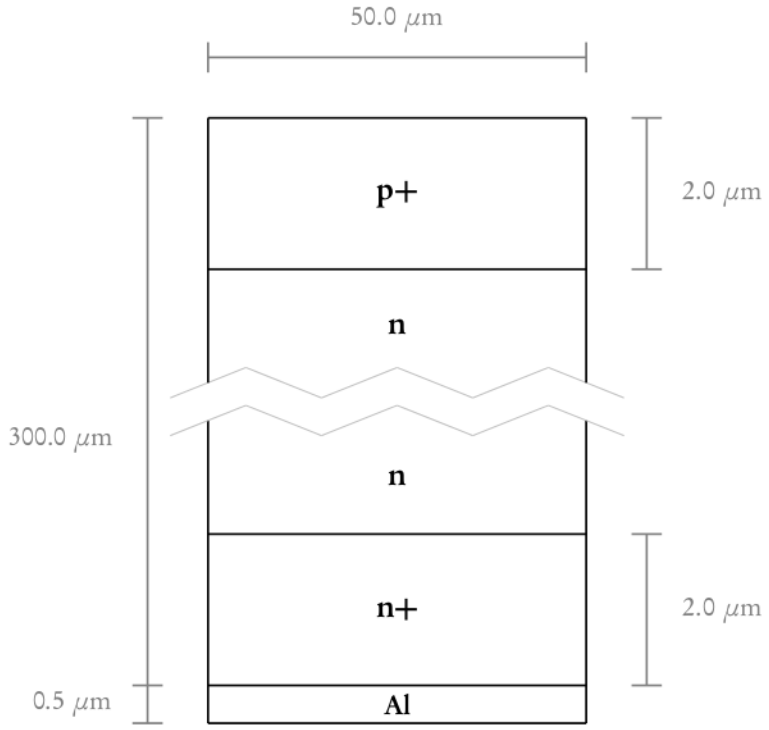

Figure 3.1: A schematic image of the simulated pn-sensor.

The simulated IV curve can be found in Fig. 3.2 along with the corresponding IV curve measured in the clean room. From this figure the depletion voltages of the simulated and real sensors can be determined, and they are found to be ~ 70 V and ~ 20 V respectively. Additionally, it is found that the two devices have similar current throughput after having depleted. The differences between the real and simulated diode that can be observed here could be attributed to the fact that the simulation was carried through with a simplified diode geometry.

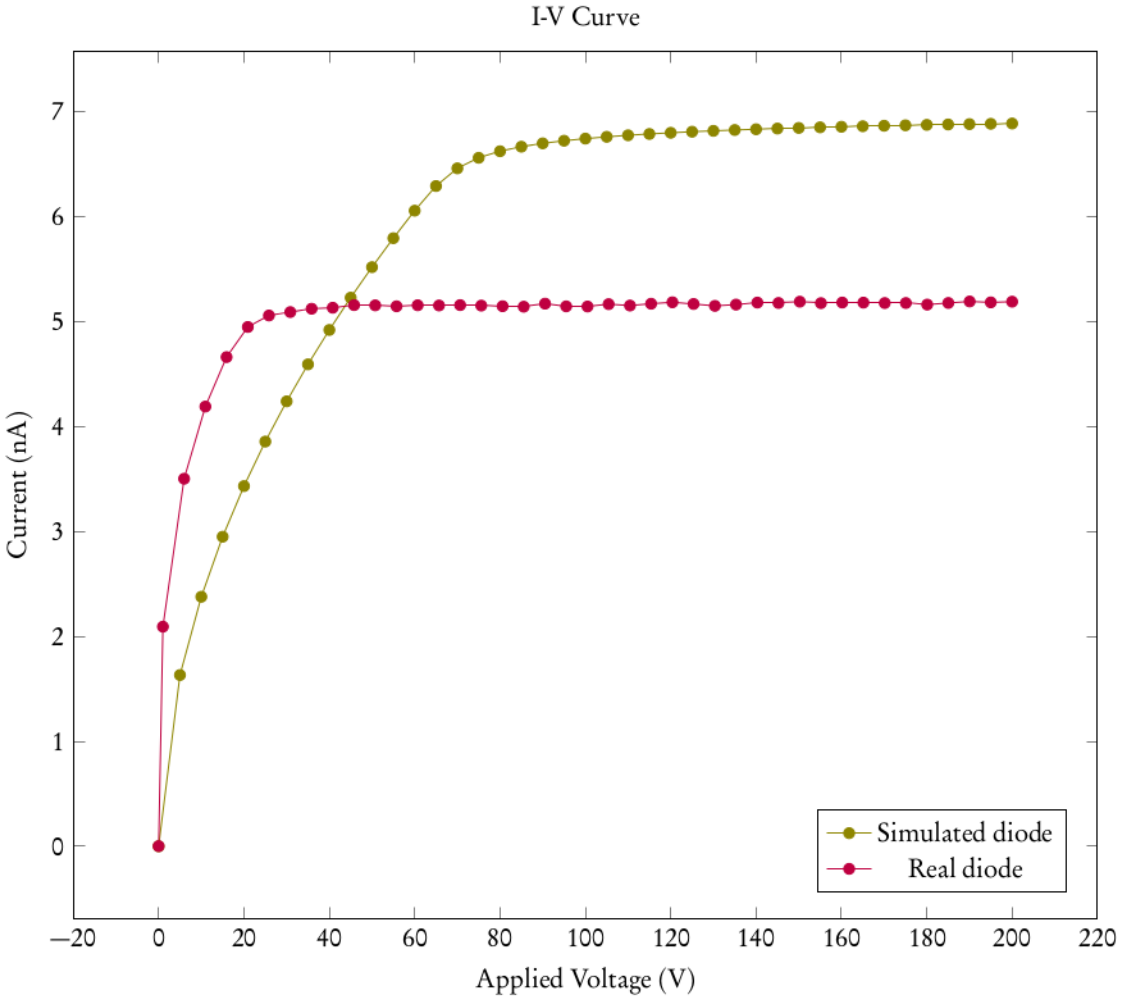

Figure 3.2: The current-voltage curve for the simulated and measured diode.

GREAT LAB RESULTS!!!

References

[1] ecee.colorado.edu/ bart/book/book

[2] semiconductors.co.uk/propiviv5431.htm

[3] nndc.bnl.gov/chart